Applied Physics Express

LETTER • **OPEN ACCESS**

Higher-order resonance of single-crystal diamond cantilever sensors toward high $f \cdot Q$ products

To cite this article: Guo Chen *et al* 2024 *Appl. Phys. Express* **17** 021001

OPEN ACCESS

Applied Physics Express 17, 021001 (2024) LETTER

https://doi.org/10.35848/1882-0786/ad2027

Higher-order resonance of single-crystal diamond cantilever sensors toward high $f \cdot Q$ products

Guo Chen[1,2], Zilong Zhang[1], Keyun Gu[1], Liwen Sang[1], Satoshi Koizumi[1], Masaya Toda[3], Haitao Ye[4], Yasuo Koide[1], Zhaohui Huang[2*], and Meiyong Liao[1*]

[1]National Institute for Materials Science, Tsukuba, Ibaraki 305-0044, Japan
[2]School of Materials Science and Technology, China University of Geosciences, Beijing 100083, People's Republic of China
[3]Graduate School of Engineering, Tohoku University, Sendai, Miyagi 980-8579, Japan
[4]School of Engineering, University of Leicester, Leicester, LE1 7RH, United Kingdom

*E-mail: huang118@cugb.edu.cn; meiyong.liao@nims.go.jp

Received December 26, 2023; revised January 15, 2024; accepted January 18, 2024; published online February 2, 2024

MEMS resonant sensing devices require both HF (f) and low dissipation or high quality factor (Q) to ensure high sensitivity and high speed. In this study, we investigate the resonance properties and energy loss in the first three resonance modes, resulting in a significant increase in $f \cdot Q$ product at higher orders. The third order resonance exhibits an approximately 15-fold increase in $f \cdot Q$ product, while the Q factor remains nearly constant. Consequently, we achieved an ultrahigh $f \cdot Q$ product exceeding 10^{12} Hz by higher-order resonances in single-crystal diamond cantilevers.

MEMS, emerging as pivotal technologies, play an increasingly vital role in a wide range of applications, from classic use like sensing, actuation, and switches in environmental monitoring, smart phones, IoT nodes, robotic servants, and autonomous vehicles to precise quantum sensors.[1–4] Resonance frequency (f) and quality (Q) factor are two fundamental parameters determining the performance of the MEMS sensors, such as response speed, detectivity, stability, and signal-to-noise ratio.[5–7] When sensing is based on the frequency shift, Q factor is of paramount importance.[8,9] However, increasing the resonance frequency always leads to the degradation of the Q factor for the fundamental resonance mode due to increased dissipation in the system.[10,11] Therefore, the product of $f \cdot Q$ presents as a figure of merit for MEMS resonators. High $f \cdot Q$ product is generally desirable to achieve high sensitivity, fast response speed, and enhanced resilience to mechanical noise sources.[11] Higher-order resonance modes have been shown promising to enhance the performance of the sensors, i.e. scanning speed and image contrast of atomic force microscope (AFM) and mass sensitivity of a cantilever.[12–14] Nevertheless, the Q factor of higher-order resonance modes is left uncontrolled.[12]

Diamond has been considered the best candidate for high-performance and high-reliability MEMS sensors in terms of its exceptional mechanical, thermal, and chemical properties.[15–18] Despite the theoretical $f \cdot Q$ of diamond in Akhieser regime is lower than Si, the practical Q factor over 1 million at room temperature was achieved, much higher than that of Si.[19,20] By using diamond cantilevers, the durability of the AFM probe and the reliability of magnetic or mass sensors under extreme conditions can be much improved.[8,13,21,22]

In this study, we investigated the higher-order resonance of single-crystal diamond (SCD) cantilevers and the $f \cdot Q$ at different resonance modes. Remarkably, with little change of the Q factors at the higher-order resonance, the $f \cdot Q$ product of the SCD increased by over 15 times, for the third order resonance relative to the first order resonance. This work provides a promising application scene for SCD MEMS cantilevers, such as AFM probes, magnetic and mass sensors.

The SCD cantilevers were fabricated using a smart-cut method from a SCD epilayer grown on an ion implanted SCD substrate, as reported previously, as shown in Fig. 1(a).[20,23] Before the fabrication of the cantilevers, a microwave plasma CVD technique was used to grow the high-quality diamond epilayer on the ion-implanted high-pressure high-temperature type-Ib SCD (100) substrate. The ion implantation was used to create a graphitized carbon layer, that would then be etched to facilitate the release of the cantilevers. During the wet-etching process, the graphite layer was removed without affecting the SCD epilayer.[24,25] Figure 1(b) shows the SCD-on-SCD structure of the fabricated diamond resonators. The SCD cantilevers had varying lengths (L) ranging from 30 to 160 μm, a thickness (t) of approximately 880 nm and a width (w) of 10 μm, as illustrated in Fig. 1(c). A 3D profile image of the MEMS cantilever distinctly depicts the upward bending, due to the existence of residual stress, as shown in Fig. 1(d). The resonance properties of the SCD cantilevers were measured in a vacuum (10^{-4} Torr) with a laser Doppler vibrometer. The SCD cantilevers were actuated by a piezoelectric ceramic or an RF probe.

We show the initial three resonance modes of a 140 μm length cantilever in Fig. 2(a). Evidently, lower-order modes exhibit larger amplitudes than higher-order modes subject to the same measurement conditions. The resonance amplitude of the first mode is 40 times greater than that of the third mode, demonstrating the increased challenge in exciting higher-order modes. The inset shows the corresponding mode shapes of the three orders. We investigated the resonance properties within the first three orders modes of SCD cantilevers. In Figs. 2(b)–2(d), we present a representative set of resonance spectra from a 140 μm length cantilever. These spectra span various orders of vibration modes, ranging from the 1st order to the 3rd order. To compare the resonance amplitudes within these higher-order modes, all measurements were performed under the same RF magnitude.

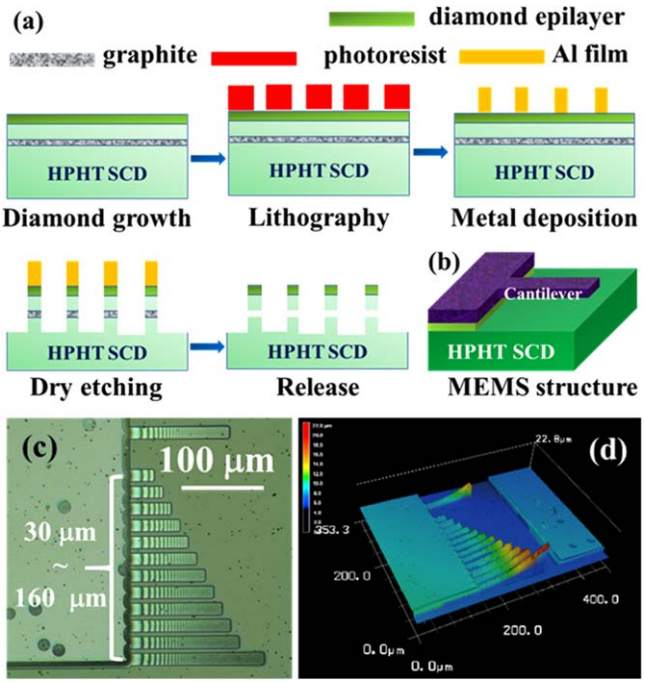

Fig. 1. (a) Fabrication process of the SCD MEMS cantilevers. (b) The structure of a SCD MEMS cantilever. (c) The optical microscope image of the SCD MEMS cantilevers. (d) The 3D geometrical profile image depicting the SCD cantilevers.

In Fig. 3, we present the dependence of the resonance frequency on the cantilever length for the first three modes. According to the Euler–Bernoulli theory, the resonance frequency of cantilevers can typically be expressed as

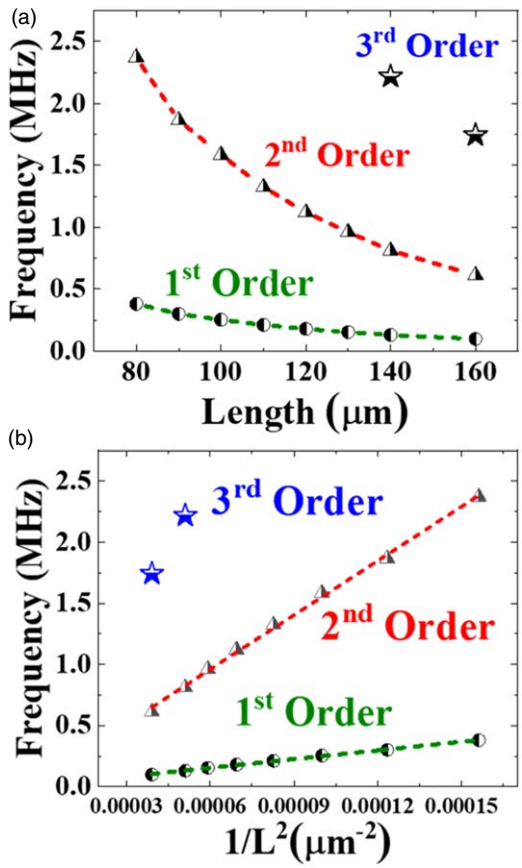

Fig. 3. (a) Dependence of the resonance frequency on the cantilever length at the first three modes. (b) The linear fit of the measured resonance frequency with $1/L^2$ for the first three modes.

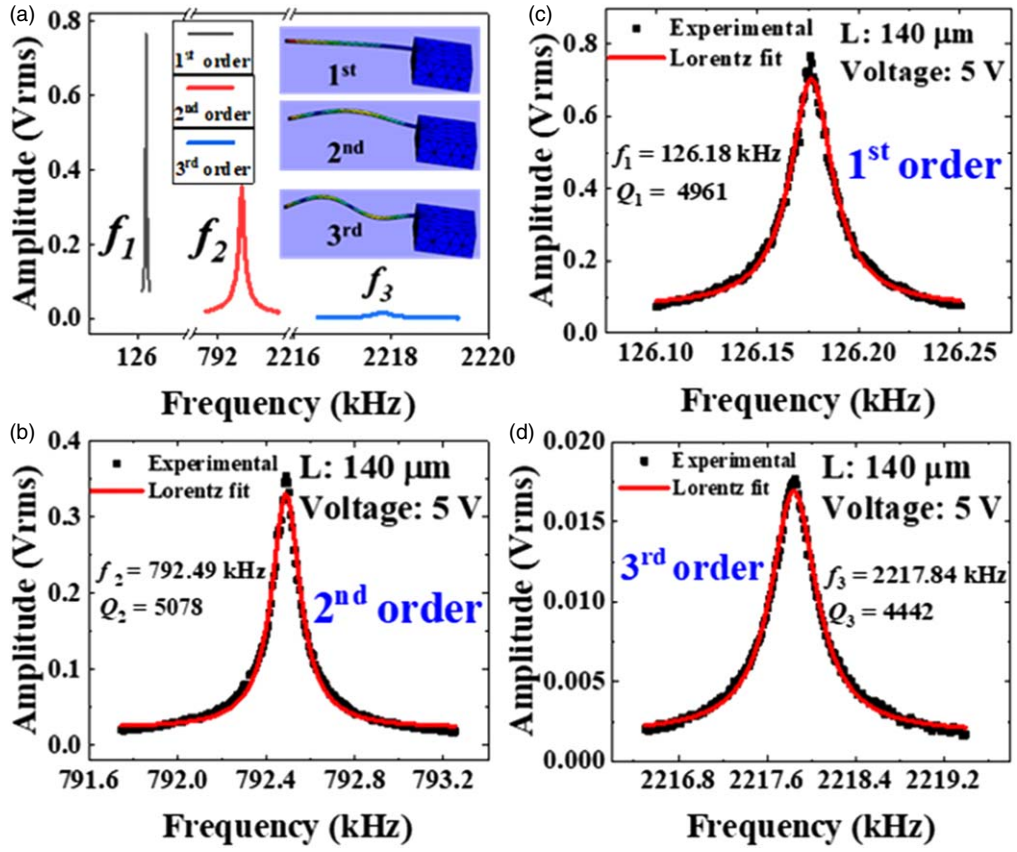

Fig. 2. Resonance frequency spectra of a SCD cantilever, under (a) the first three orders, and individually at the (b) 1st, (c) 2nd, (d) 3rd order mode.

$$f_n = \frac{\omega_n}{2\pi} = \frac{\lambda_n^2 t}{2\pi L^2}\sqrt{\frac{E}{12\rho}} = k_n \frac{t}{L^2}\sqrt{\frac{E}{\rho}}, \quad (1)$$

where n refers to the vibration mode number. λ takes values of 1.875, 4.694, 7.855, $(2n-1)\,\pi/2 \cdots (n = 1, 2, 3, n > 3 \cdots)$. $k_1 = 0.162$, $k_2 = 1.012$, and $k_3 = 2.835$. ω, E, L, t, and ρ represent the angular resonance frequency, Young's modulus, cantilever length, thickness, and mass density, respectively.[26,27] For the SCD cantilever in this study, $E = 1100$ GPa and $\rho = 3.5$ g cm^{-3}, respectively. As revealed in Fig. 3, the variation of the resonance frequency versus length exhibits remarkable consistency between experimental and theoretical results for all the three modes.

Higher-order modes are pursued in AFM imaging, which are more sensitive to the position of the probe, an additional mass, and application of force.[28] In the meantime, the Q factor determines the image resolution and resonance amplitude. Therefore, optimizing the $f{\cdot}Q$ product is of critical importance that directly influences the measurement band width and vibration amplitude.[29] We obtained the Q factors by using the band width method through a Lorentzian fitting of the frequency spectra. We show the relationship between the cantilever length and both Q factor and $f{\cdot}Q$ product, respectively, as presented in Fig. 4(a). Significantly, the $f{\cdot}Q$ product for higher-order vibrations remarkably exceeds that of the fundamental mode. Furthermore, the $f{\cdot}Q$ product exhibits a decrease with an increase in cantilever length due to the reduction in resonance frequency. A comparative assessment of the Q factor and $f{\cdot}Q$ product in the first three modes is depicted in Fig. 4(b). It becomes apparent that the $f{\cdot}Q$ for the SCD cantilevers experiences a substantial increase with higher-order resonances. Specifically, the third order mode exhibits a $f{\cdot}Q$ value of approximately $\sim 10^{10}$ Hz, marking a nearly fifteen-fold enhancement compared to the first order mode. However, due to the ion-implantation induced defects in the diamond cantilever, the Q factor is similar for different resonance orders. This highlights that the $f{\cdot}Q$ value is greatly enhanced through the utilization of higher-order resonance modes.

We investigated the dissipation mechanisms of the higher-order resonance modes. Since the measurements were conducted in high vacuum environment, the air damping is neglected. The overall Q factor is determined by the following diverse dissipation mechanisms

$$Q^{-1} = Q_{\text{clamp}}^{-1} + Q_{\text{TED}}^{-1} + Q_{\text{MD}}^{-1} + Q_{\text{surface}}^{-1}, \quad (2)$$

where clamp, TED, MD, and surface signify the Q factors attributed to the energy loss mechanisms of clamping losses, thermoelastic damping, mechanical defects, and surface loss, respectively.[30,31] Higher-order resonances are shown to suffer less from clamping loss compared to the fundamental mode.[31] This is possibly because higher-order resonances store a larger amount of mechanical energy at nodes that are situated farther away from the clamping points.[32] Thermoelastic loss does not dominate due to Q_{TED} exceeding 10^7 at room temperature.[33] The crystal quality of diamond affects the Q factor of the diamond cantilevers.[25,34] In our case, we disclosed that the diamond cantilever has single-crystal nature by high-resolution transmission electron microscope.[20] However, considering that the smart-cut method for the SCD cantilever fabrication involves a high-energy ion implantation, the ion-irradiated defects determine the ultimate

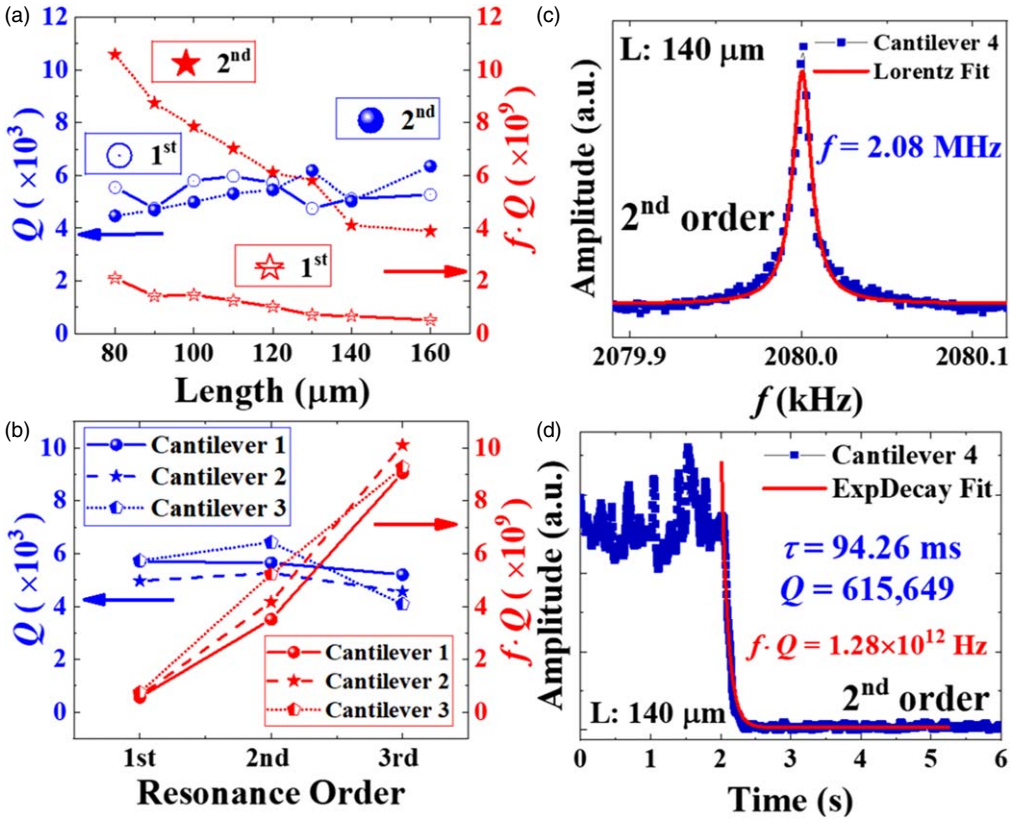

Fig. 4. Dependence of Q and $f{\cdot}Q$ on cantilever lengths (a), resonance orders (b), for diamond cantilever 1–3. (c) Resonance frequency spectrum, and (d) ring-down measurement of diamond cantilever 4 at the 2nd order.

Q factor. In this work, surface loss can be included in the mechanical defects loss due to ion-implantation induced defective layer at the bottom of the SCD cantilevers.[20] Therefore, the relatively low Q factor can be attributed to defects induced by ion damage. By harnessing higher mode resonance, we are able to achieve the $f{\cdot}Q$ product comparable to that of the SCD cantilevers fabricated using the transfer technique, which boosts a Q factor exceeding 1 million.[19] This enhancement of $f{\cdot}Q$ was achieved without the need for additional materials processing such as prolonged annealing or etching.[20,35]

Based on the discussion described above, we fabricated a higher Q factor diamond resonator (cantilever 4), by removing the defects within the cantilevers based on the atomic scale etching.[20] The resonance frequency of the 1st order mode is 342.14 kHz and the 2nd order is 2.08 MHz. In Fig. 4(c), the resonance frequency spectrum of cantilever 4 in the 2nd order mode is presented. Since the resonance frequency of the 3rd order mode is out of the limit (3 MHz) of the setup, we solely present data for the 2nd order mode. To achieve greater accuracy beyond the frequency resolution limit, we employed ring-down measurements to obtain the Q factors. These Q factors were then calculated by $Q = \pi\tau f$, where τ represents the characteristic decay time of the resonator. The ring-down plots in Fig. 4(d) illustrate a decay time of 94.26 ms and an ultrahigh Q factor over 6×10^5 in the 2nd order resonance. Remarkably, we achieved a high $f{\cdot}Q$ product over 10^{12} Hz for the 2nd order mode. This value is the highest in SCD cantilevers up to date.[36]

In conclusion, we investigated the higher-order resonances in SCD cantilevers. The resonance frequency of diamond cantilevers remained consistent in both experiment and theory under higher-order modes. Despite the low Q factor dominated by the crystal defects within the cantilever, the $f{\cdot}Q$ product was remarkably improved by over 15 times related to the fundamental mode resonance. We achieved an unprecedented ultrahigh $f{\cdot}Q$ product over 10^{12} Hz within a higher-order resonance mode of a SCD cantilever.

Acknowledgments This work was supported by JSPS KAKENHI (Grant Nos. 20H02212, 22K18957, 15H03999), Bilateral joint research between JSPS/CAS, Advanced Research Infrastructure for Materials and Nanotechnology in Japan (ARIM) of MEXT (JPMXP1223NM5297), and European Union's Horizon 2020 Marie Skłodowska-Curie project (GA No 101027489). Guo Chen thanked to financial support from China Scholarship Council (No. 202006400023).

ORCID iDs Meiyong Liao https://orcid.org/0000-0003-1361-4266

1) H. Sun, X. Shen, L. Sang, M. Imura, Y. Koide, J. You, T.-F. Li, S. Koizumi, and M. Liao, Appl. Phys. Express **14**, 045501 (2021).
2) Z. Zhang, G. Chen, K. Gu, S. Koizumi, and M. Liao, Funct. Diam. **3**, 2221280 (2023).
3) R. Hajare, V. Reddy, and R. Srikanth, Mater. Today Proc. **49**, 720 (2022).
4) H. Sun, Z. Zhang, Y. Liu, G. Chen, T. Li, and M. Liao, Adv. Quantum Technol. **6**, 2300189 (2023).
5) T. Yamada, Y. Ando, H. Watanabe, Y. Furusawa, A. Tanaka, M. Deki, S. Nitta, Y. Honda, J. Suda, and H. Amano, Appl. Phys. Express **14**, 036505 (2021).
6) Y. Zhang, Y. Yoshioka, I. Morohashi, and X. Liu, Appl. Phys. Express **14**, 014001 (2020).
7) M. Liao, M. Toda, L. Sang, T. Teraji, M. Imura, and Y. Koide, Jpn. J. Appl. Phys. **56**, 024101 (2017).
8) Z. Zhang, W. Zhao, G. Chen, M. Toda, S. Koizumi, Y. Koide, and M. Liao, Adv. Funct. Mater. **33**, 2300805 (2023).
9) U. Soysal, F. Marty, E. Géhin, C. Motzkus, and E. Algré, Microelectron. Eng. **221**, 111190 (2020).
10) M. Liao, M. Toda, L. Sang, S. Hishita, S. Tanaka, and Y. Koide, Appl. Phys. Lett. **105**, 251904 (2014).
11) M. Imboden and P. Mohanty, Phys. Rep. **534**, 89 (2014).
12) S. I. Moore, M. G. Ruppert, and Y. K. Yong, Int. Conf. on Manipulation, Automation and Robotics at Small Scales (MARSS), 2018, p. 1.
13) A. N. Obraztsov, P. G. Kopylov, B. A. Loginov, M. A. Dolganov, R. R. Ismagilov, and N. V. Savenko, Rev. Sci. Instrum. **81**, 013703 (2010).
14) D. Jin, X. Li, J. Liu, G. Zuo, Y. Wang, M. Liu, and H. Yu, J. Micromech. Microeng. **16**, 1017 (2006).
15) O. Auciello, S. Pacheco, A. V. Sumant, C. Gudeman, S. Sampath, A. Datta, R. W. Carpick, V. P. Adiga, P. Zurcher, and Z. Ma, IEEE Microwave Mag. **8**, 61 (2007).
16) M. Liao, L. Sang, H. Sun, T. Li, and S. Koizumi, Appl. Phys. Lett. **119**, 073504 (2021).
17) M. Liao, Funct. Diam. **1**, 29 (2022).
18) H. Deguchi, T. Hayashi, H. Saito, Y. Nishibayashi, M. Teramoto, M. Fujiwara, H. Morishita, N. Mizuochi, and N. Tatsumi, Appl. Phys. Express **16**, 062004 (2023).
19) Y. Tao, J. M. Boss, B. A. Moores, and C. L. Degen, Nat. Commun. **5**, 3638 (2014).
20) H. Wu, L. Sang, Y. Li, T. Teraji, T. Li, M. Imura, J. You, Y. Koide, M. Toda, and M. Liao, Phys. Rev. Mater. **2**, 090601 (2018).
21) T. Hantschel, S. Slesazeck, P. Niedermann, P. Eyben, and W. Vandervorst, Microelectron. Eng. **57**, 749 (2001).
22) A. Ghosh, C. Zhang, S. Q. Shi, and H. Zhang, CLEAN—Soil, Air, Water **47**, 1800491 (2019).
23) M. Liao, S. Hishita, E. Watanabe, S. Koizumi, and Y. Koide, Adv. Mater. **22**, 5393 (2010).
24) M. Liao, Z. Rong, S. Hishita, M. Imura, S. Koizumi, and Y. Koide, Diam. Relat. Mater. **24**, 69 (2012).
25) O. Auciello and D. M. Aslam, J. Mater. Sci. **56**, 7171 (2021).
26) W. Weaver, S. P. Timoshenko, and D. H. Young, *Vibration Problems in Engineering* (Wiley, New York, 1991).
27) H. A. C. Tilmans, M. Elwenspoek, and J. H. J. Fluitman, Sens. Actuators A **30**, 35 (1992).
28) Y. M. Tseytlin, Rev. Sci. Instrum. **79**, 025102 (2008).
29) M. Faucher, B. Walter, A.-S. Rollier, K. Seguini, B. Legrand, G. Couturier, J.-P. Aimé, C. Bernard, R. Boisgard, and L. Buchaillot, TRANSDUCERS 2007-2007 Int. Solid-State Sensors, Actuators and Microsystems Conf., 2007, p. 1529.
30) Z. Hao, A. Erbil, and F. Ayazi, Sens. Actuators, A **109**, 156 (2003).
31) J. M. L. Miller, A. Ansari, D. B. Heinz, Y. Chen, I. B. Flader, D. D. Shin, L. G. Villanueva, and T. W. Kenny, Appl. Phys. Rev. **5**, 041307 (2018).
32) A. Gaidarzhy, M. Imboden, P. Mohanty, J. Rankin, and B. W. Sheldon, Appl. Phys. Lett. **91**, 203503 (2007).
33) H. Sun, L. Sang, H. Wu, Z. Zhang, T. Teraji, T.-F. Li, J. You, M. Toda, S. Koizumi, and M. Liao, Phys. Rev. Lett. **125**, 206802 (2020).
34) A. V. Sumant, O. Auciello, M. Liao, and O. A. Williams, MRS Bull. **39**, 511 (2014).
35) G. Chen, Z. Zhang, Y. Koide, S. Koizumi, Z. Huang, and M. Liao, Diam. Relat. Mater. **138**, 110240 (2023).
36) Y.-I. Sohn, M. J. Burek, V. Kara, R. Kearns, and M. Lončar, Appl. Phys. Lett. **107**, 243106 (2015).